Article

Evidence for the I-Shaped Dimers of a Plant Chloroplast F_OF_1-ATP Synthase in Response to Changes in Ionic Strength

Stepan D. Osipov , Yury L. Ryzhykau , Egor V. Zinovev , Andronika V. Minaeva , Sergey D. Ivashchenko , Dmitry P. Verteletskiy , Vsevolod V. Sudarev , Daria D. Kuklina , Mikhail Yu. Nikolaev , Yury S. Semenov , Yuliya A. Zagryadskaya , Ivan S. Okhrimenko , Margarita S. Gette , Alexander I. Kuklin , Valentin Ivanovich , Vladimir N. Uversky * , Alexey V. Vlasov *

Posted Date: 4 May 2023

doi: 10.20944/preprints202305.0170.v1

Keywords: FOF1-ATP synthase; chloroplasts; dimers; small-angle scattering; membrane proteins

Article

Evidence for the I-Shaped Dimers of a Plant Chloroplast F_OF_1-ATP Synthase in Response to Changes in Ionic Strength

Stepan D. Osipov [1,†], Yury L. Ryzhykau [1,2,†], Egor V. Zinovev [1], Andronika V. Minaeva [1], Sergey D. Ivashchenko [1], Dmitry P. Verteletskiy [3], Vsevolod V. Sudarev [1], Daria D. Kuklina [1], Mikhail Yu. Nikolaev [1], Yury S. Semenov [1], Yuliya A. Zagryadskaya [1], Ivan S. Okhrimenko [1], Margarita S. Gette [1], Alexander I. Kuklin [1,2], Valentin Ivanovich [1], Vladimir N. Uversky [4,*] and Alexey V. Vlasov [1,2,*]

[1] Research Center for Mechanisms of Aging and Age-Related Diseases, Moscow Institute of Physics and Technology, Dolgoprudny, 141700, Russian Federation
[2] Frank Laboratory of Neutron Physics, Joint Institute for Nuclear Research, Dubna, 141980, Russian Federation
[3] Mainchemproject South, LLC, Yerevan, Armenia
[4] Department of Molecular Medicine and Byrd Alzheimer's Research Institute, Morsani College of Medicine, University of South Florida, Tampa, FL, USA
* Correspondence: aleksei.vlasov@phystech.edu (A.V.V.); vuversky@usf.edu (V.N.U.)
† Equal contribution.

Abstract: F-type ATP synthases play a key role in oxidative and photophosphorylation processes producing adenosine triphosphate (ATP) for most biochemical reactions in living organisms. In contrast to the mitochondrial F_OF_1-ATP synthases those of chloroplasts are known to be mostly monomers with approx. 15% fraction of oligomers interacting presumably non-specifically in a thylakoid membrane. To shed light to the nature of this difference we studied interactions of the chloroplast ATP synthases using small-angle X-ray scattering (SAXS) method. Here, we report evidence of I-shaped dimerization of solubilized F_OF_1-ATP synthases from spinach chloroplasts at different salinity. The structural data were obtained by SAXS and showed dimerization in response to changes in ionic strength. The best model describing SAXS data was two ATP-synthases connected through F_1/F_1' parts, presumably via their δ-subunits, forming dimers with the "I" shape. Such I-shaped dimers might possibly connect the neighboring lamellae in thylakoid stacks assuming that the F_OF_1 monomers comprising such dimers are embedded in different thylakoid membranes. If this type of dimerization exists in nature, it might be one of the pathways of inhibition of chloroplast F_OF_1-ATP synthase for preventing of ATP hydrolysis in dark, when salinity in plant chloroplasts is rising. Together with a redox switch inserted into a γ-subunit of chloroplast F_OF_1 and lateral oligomerization, an I-shaped dimerization might comprise a subtle regulatory process of ATP synthesis and stabilize the structure of thylakoid stacks in chloroplasts.

Keywords: F_OF_1-ATP synthase; chloroplasts; dimers; small-angle scattering; membrane proteins.

1. Introduction

The ATP synthase is the object of intensive studies for at least half a century. This interest is defined by the fact that the enzyme provides cells with adenosine triphosphate (ATP), which is the key molecule for almost all biochemical reactions in living organisms, being the major source of energy for use and storage at the cellular level. F-type ATP synthases were found in mitochondria of eukaryotes, bacterial cellular membranes, and chloroplasts. ATP synthase couples transmembrane ion transport, established by mechanical rotation of a c-ring in a membrane (F_O) region, with conformational changes in ATP catalytic centers at α/β interfaces (F_1 region).

In mitochondria cristae, ATP synthases (mtF_OF_1) were found to form dimers of four different types (V-shape dimers of types I, II and IV, and U-shape dimer of a type III) [1]. In contrast, in bacteria, ATP synthases (bF_OF_1) are known to be monomers [2]. ATP synthases in thylakoid membranes (cF_OF_1)

 doi:10.20944/preprints202305.0170.v1

were shown to be primarily monomeric with approx. 12% fraction of dimers and 3% of higher oligomers [3]. According to what is known, the contacts between two cF$_O$F$_1$ monomers are highly-likely non-specific, and such dimerization might inhibit ATP synthases, preventing ATP hydrolysis in the absence of photosynthesis.

A dimerization of cF$_O$F$_1$ might be induced by changing of ionic strength in plant chloroplast during the light/dark switches. The internal volume of a chloroplast is separated from a cytoplasm by a lipid membrane, which, together with the pumps and channels, makes it possible to create and maintain a difference between ion concentration inside and outside the chloroplast. This difference can vary significantly from species to species, and between some organisms it can reach more than ten times values [4]. It is known that under light, various ions are redistributed in plants. The phenomenon of light-induced uptake of hydrogen ions by isolated chloroplasts is well studied. It is accompanied by the redistribution of other ions, such as Na, K, Cl, and Mg, implying that the ionic strength of the solution contained in plant chloroplasts can change 1.5 times during the day [5,6].

SAXS is an excellent structural method to study biological macromolecules in solutions; i.e., it allows one to perform the studies under variety of conditions, including different ionic strengths. In our work, we report an evidence of the *in vitro* dimerization of cF$_O$F$_1$ in response to increasing ionic strength. The structural data were obtained by SAXS measurements of solubilized and purified samples of cF$_O$F$_1$ from spinach chloroplasts at different NaCl concentrations. SAXS data analysis resulted in a model of an I-shaped dimer of cF$_O$F$_1$, which in a mixture with monomeric cF$_O$F$_1$, provided the best fit of the experimental data. I-shaped cF$_O$F$_1$ dimer is formed by F$_1$/F$_1$ contacts, presumably via δ/δ subunit interaction, so that the F$_O$ parts of the monomers are on the opposite sides of the dimer. We used a macromolecular docking to refine our model and improved the quality of the fit of SAXS data for each NaCl concentration thereby generating a high-resolution model of these dimers.

Therefore, we present here a new model of a dimer of F-ATP synthases from spinach chloroplasts, which has a specific F$_1$/F$_1$ interaction, presumably via δ-subunits. We speculate that changing of ionic strength in plant chloroplasts during the day (light/dark period of time) might trigger the formation of cF$_O$F$_1$ oligomers in chloroplasts and, in particular, I-shaped cF$_O$F$_1$ dimers. We hypothesize that chloroplast ATP synthases might also form oligomers in order to inhibit ATP hydrolysis at dark, and I-shaped dimers might possibly connect the neighbor lamellae and stabilize thylakoid stacks in chloroplasts.

The reported here model of the cF$_O$F$_1$ I-shaped dimer is unexpected, and raises questions whether such type of dimerization exists in nature. First, such dimer should be inserted in two membranes at a specific distance from each other. Second, it should change the rate of ATP synthesis due to steric hindrance of δ-subunits.

2. Results

2.1. Purification of the monomeric F$_O$F$_1$ ATP-synthase from thylakoid membranes

Isolation and purification of cF$_O$F$_1$ from spinach chloroplasts was conducted as described [7–9], and the final step of purification utilized treatment with a detergent 4-trans-(4-trans-Propylcyclohexyl)-cyclohexyl α-maltoside (t-PCCαM) followed by the anion exchange chromatography (AEX) against the NaCl concentration gradient (50 – 1000 mM) (Figure 1a). The AEX chromatogram showed a peak at ~300mM NaCl (Figure 1b), which corresponds to the whole cF$_O$F$_1$ protein complex according to SDS-PAGE (Figure 1c). Blue-Native PAGE was also used to check the completeness and assembly of cF$_O$F$_1$ (Figure S1).

Preprints (www.preprints.org) | NOT PEER-REVIEWED | Posted: 4 May 2023 doi:10.20944/preprints202305.0170.v1

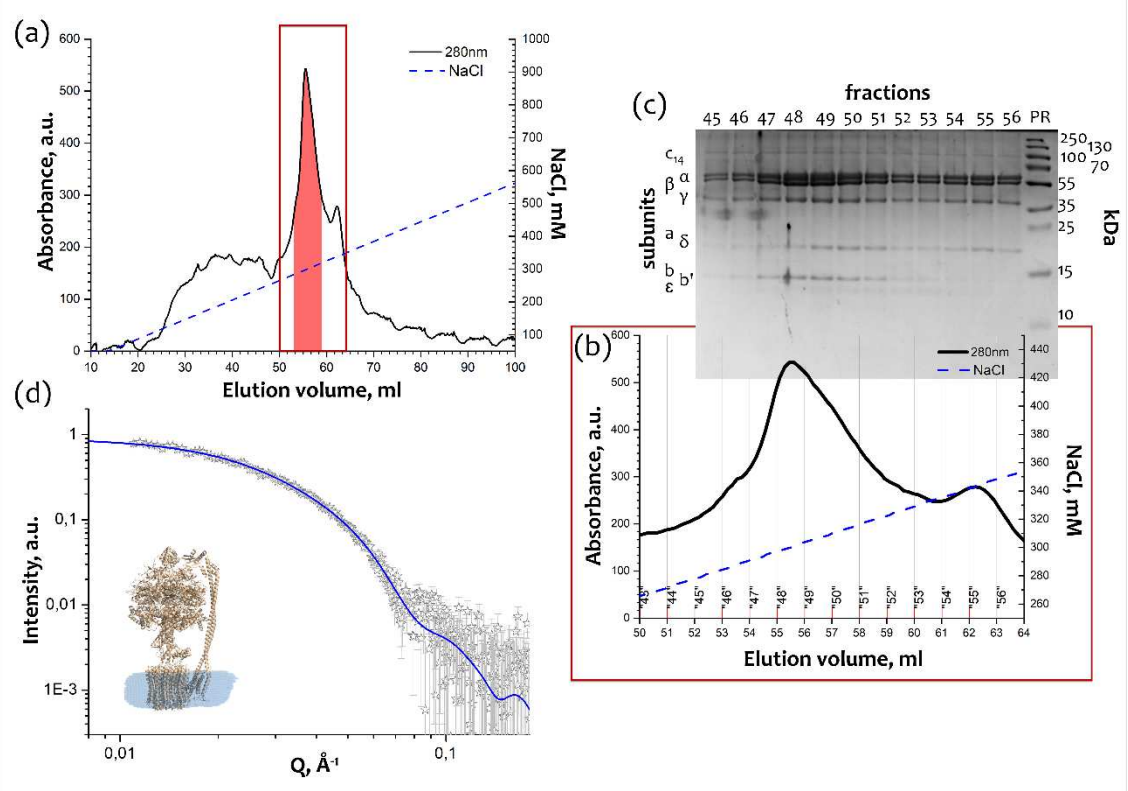

Figure 1. Purification and characterization of cFoF1: (**a**) Anion exchange chromatography (AEX) of cFoF1 from spinach chloroplasts, highlighted fractions were merged and taken for structural studies; (**b**) AEX peak fractions of cFoF1; (**c**) Characterization of the AEX peak fractions of cFoF1 by SDS PAGE; (**d**) Characterization of the AEX peak fractions of cFoF1 by SAXS, experimental I(Q) 1D-profile showed as hollow grey stars, a model of cFoF1 (PDB ID: 6FKF) with a detergent belt was used for approximation of experimental data with χ^2 = 1.15 (blue line). Panels (a), (b) and (c) were adapted from [7] with modifications.

The peak fractions of cFoF1 were measured by SAXS and showed a good consistensy (χ^2 = 1.15) with the monomeric model of chloroplast ATP-synthase (PDB ID: 6FKF [10]) with a detergent belt built by MEMPROT program [11] (Figure 1d). Despite the fact that for membrane proteins solubilized in detergent, including large protein complexes, the presence of the local maxima at 0.1 – 0.2 Å^{-1} is common for their I(Q) SAXS profile [12,13], our experiments and literature data obtained for an A-type ATP-synthse (SASBDB ID: SASDKK4) [14] show that it is not a rule even for different ATP-synthases. Nevertheless, taking into account a detergent belt allows improving the χ^2 from 1.35 to 1.15 (Figure S3).

2.2. SAS studies of cFoF1 dimerization at different NaCl concentrations

When investigating the samples of purified cFoF1 by small-angle neutron scattering (SANS) at 93% D_2O, 300 mM NaCl the increase of the maximum size and a radius of gyration (Rg) for the samples were more than expected from a contrast variation technique (Figure S2). This effect might have pointed towards an increase of an average oligomeric state in the sample, i.e. oligomerization polidispersity [12]. We hypothesized that a change of ionic strength could have led to oligomerization of cFoF1. In order to verify this hypothesis, we measured samples of purified cFoF1 at a range of NaCl concentrations by small-angle X-ray scattering (SAXS) (Figure 2a).

Preprints (www.preprints.org) | NOT PEER-REVIEWED | Posted: 4 May 2023 doi:10.20944/preprints202305.0170.v1

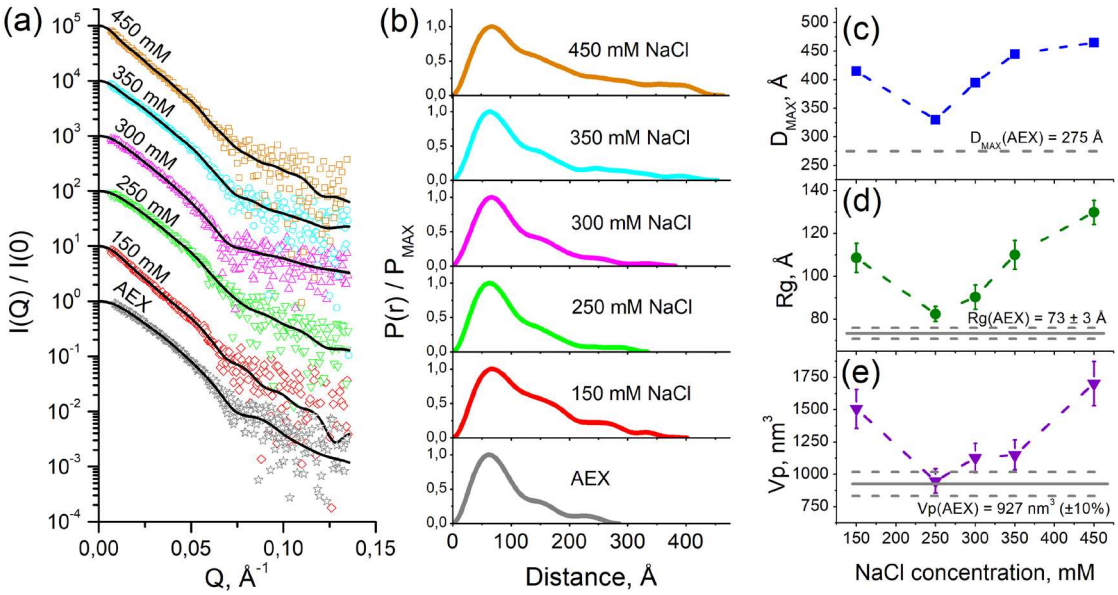

Figure 2. SAXS characterization of cFoF1: (**a**) Experimental I(Q) 1D-profiles for AEX-purified and dialyzed against different NaCl concentrations samples of cFoF1, experimental data is shown as dots, regularized fits are shown as black lines. For clarity, SAXS data for 150, 250, 300, 350 and 450 mM NaCl were multiplied by 10, 10^2, 10^3, 10^4, and 10^5, respectively; (**b**) Normalized pair-distance distribution function P(r) for cFoF1 at different NaCl concentrations; (**c**) Maximum size of the object (D_{max}) for samples of cFoF1 at different NaCl concentrations; (**d**) Radius of gyration (Rg) for samples of cFoF1 at different NaCl concentrations obtained from P(r); (**e**) Porod volume (Vp) for samples of cFoF1 at different NaCl concentrations. Gray lines show the values of D_{max}, Rg, Vp for an AEX-purified sample of cFoF1 without dialysis. The values used for plots in panels (**c** – **e**) are given in Table S1.

It is worth to mention that all samples of cFoF1 were first purified at the same conditions and after AEX the buffer contained 30 mM HEPES (pH 8.0), 2 mM $MgCl_2$, 250 – 300 mM NaCl, 0.04 % (w/v), tPCC-α-M (4-trans-(4-trans-Propylcyclohexyl)-cyclohexyl α-maltoside). Then, the samples were dialyzed against different NaCl concentrations (150, 250, 300, 350, 450 mM) and after dialysis they were measured by SAXS.

Pair-distance distribution function P(r) for samples of cFoF1 at different NaCl concentrations (Figure 2b) showed the increase of maximum size of the object D_{max} (Figure 2c), radius of gyration Rg (Figure 2d), and Porod volume Vp (Figure 2e) with changing of ionic strength, reaching the maxima at 150 and 450 mM NaCl and the minimum at 250 – 300 mM NaCl. It implies the increase of oligomerization fraction in the samples with both a decrease and an increase of ionic strength.

The most certainly a dimerization of cFoF1 was observed for the least and the most salinity from investigated range (150 and 450 mM NaCl, respectively). The distance between two monomers of cFoF1 in the dimer can be estimated as following:

$$D_{m-m} = 2\sqrt{\frac{1+\alpha}{2\alpha}\left(Rg_{mix}^2 - Rg_{mono}^2\right)}, \quad (1)$$

where Rg_{mono} and Rg_{mix} are radii of gyration for monomeric ATP-synthase and average for monomer-dimer mixure, correspondingly, α is a volume fraction of dimers estimated as $\alpha = Vp_{mix}/Vp_{mono}$. Considering Vp errors as 10% and Rg errors (see Table S1) we estimate D_{m-m} equals to 183 ± 30 Å and 225 ± 24 Å for 150 mM and 450 mM NaCl, correspondingly.

The discrepancy of the values D_{m-m} might indicate different dimerization mechanisms at low and high salinity. Nevertheless, such values of D_{m-m} (similar to the size of cFoF1) imply that the contacts between two monomers of cFoF1 are at the edge of these protein complexes. Thus, only two types of contacts are possible: Fo/Fo (presumably via c-ring) or F1/F1 (presumably via δ-subunit).

Preprints (www.preprints.org) | NOT PEER-REVIEWED | Posted: 4 May 2023 doi:10.20944/preprints202305.0170.v1

2.3. Models of an I-shaped cFoF1 dimer

Taking into account the fact that the oligomerization increases at changing the ionic strength and the possible types of contacts derived from the $D_{m\text{-}m}$ value, we built two models of cFoF1 which satisfy these conditions. In the first case, we built a model comprising a mixture of a monomeric cFoF1 and dimers with Fo/Fo contacts, presumably via c-ring (Figure 3a). In the second case, a model comprises a mixture of a monomeric cFoF1 and dimers with F1/F1 contacts, presumably via δ-subunit (Figure 3b).

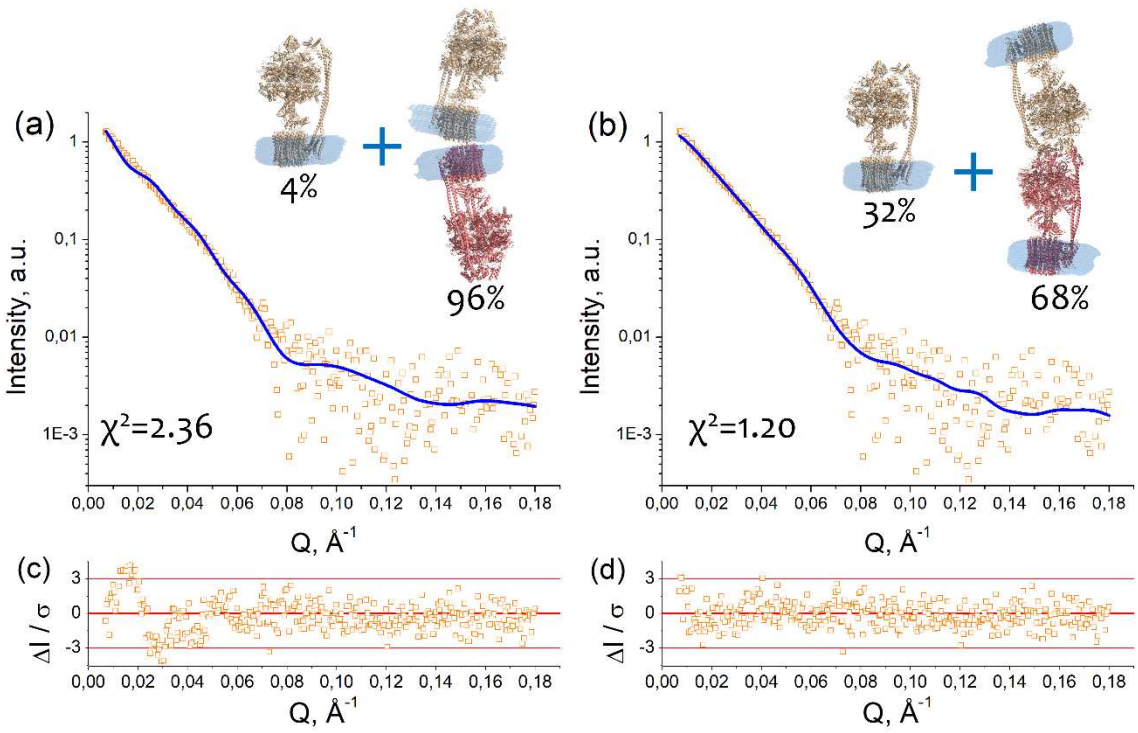

Figure 3. Dimerization of cFoF1 from Spinacia oleracea at 450 mM NaCl shown by SAXS: (**a**) Experimental I(Q) 1D-profile for cFoF1 at 450 mM NaCl (orange squares) and an approximation (blue line, $\chi^2 = 2.36$) by using a model of a mixture of cFoF1 monomers and dimers formed by Fo-Fo contacts (see *Macromolecular docking* section in Materials and Methods); (**b**) Experimental I(Q) 1D-profile for cFoF1 at 450 mM NaCl (the same as in panel (**a**), orange squares) and an approximation (blue line, $\chi^2 = 1.20$) by using a model of a mixture of cFoF1 monomers and dimers formed by F1-F1 contacts (see *Macromolecular docking* section in Materials and Methods); (**c**) Relative residues of the fit shown in panel (**a**); (**d**) Relative residues of the fit shown in panel (**b**). The models of monomeric and dimeric cFoF1, shown in panels (**a**) and (**b**), contain detergent belts obtained by the program MEMPROT. Volume fractions of monomers and dimers of cFoF1, used in the models for approximation, are shown.

The models of monomeric and dimeric cFoF1 contain detergent belts obtained by a program MEMPROT for the monomeric AEX fraction (see Figure 1d). The models of cFoF1 dimers were constructed using HDOCK protein–protein docking web-server [15]. Two types of restraints have been used, providing Fo/Fo or F1/F1 contacts, as described in *Macromolecular docking* section in Materials and Methods.

An approximation of SAXS data with these models resulted in $\chi^2 = 2.36$ in the case of Fo/Fo dimers and $\chi^2 = 1.20$ for F1/F1 dimers with a fraction of dimeric cFoF1 96 ± 3 % and 68 ± 2 % for Fo/Fo and F1/F1 dimers, respectively (Figure 3a, b). The approximation by the model containing F1/F1 dimers showed better χ^2 value and relative residues $\Delta I/\sigma$ at small Q, which are within 3 (Figure 3d), in contrast to the approximation by the model containing Fo/Fo dimers (Figure 3c). Therefore, the model

 doi:10.20944/preprints202305.0170.v1

comprising a mixture of a monomeric cF_OF_1 and dimers with F_1/F_1 contacts, presumably via δ-subunit, showed the best fit of the SAXS data.

In the case of the cF_OF_1 dimers with F_O/F_O contacts, D_{m-m} values for top 10 HDOCK predictions (see *Macromolecular docking* section in Materials and Methods for details) were in the range of 174 – 201 Å. The only model (Figure 3a), which has $D_{m-m} \geq 201$ Å (a lower limit of the range 225 ± 24 Å) (eq. 1), resulted in $\chi^2 = 2.36$ and a fraction of dimers ~96 % for fitting of SAXS data for purified cF_OF_1 samples at 450 mM NaCl.

In the case of the cF_OF_1 dimers with F_1/F_1 contacts, D_{m-m} values for top 10 HDOCK predictions (see *Macromolecular docking* section in Materials and Methods for the details) were in the range of D_{m-m} 150 – 210 Å. All of these models, including one shown in Figure 3b (Model 4 in Figure S4), in addition to contacts between δ-subunits, demonstrated contacts between other subunits, including α-, β-, b- and b'-subunit. Five out of ten models have $D_{m-m} \geq 201$ Å and demonstrated χ^2 values in the range of 1.16 – 1.20 (see details in Figure S4) for fitting SAXS data for purified cF_OF_1 samples at 450 mM NaCl. Figure 3b shows one of these five models which corresponds to the best HDOCK confidence score (Figure S4). An additional validation of parameters of macromolecular interfaces estimated using the PDBePISA web-server [16] allowed us to asses this model as reasonable both in terms of HDOCK confidence score values and PDBePISA metric (see Figure S4 for the details).

2.4. A possible physiological role of I-shaped cF_OF_1 dimers

Concerning a physiological relevance, we hypothesize that I-shaped type of dimerization might stabilize the stacks of chloroplasts by possible connection of neighboring lamellae. It is known that a large number of ATP-synthases is located in stroma lamellae and grana membranes [3,17] (Figure 4a). High density of molecules in these membranes leads to formation of contacts between them and lateral dimerization (Figure 4b). At the same time, the distance between neighboring stroma lamellae is about 30 nm, which approximately fits the I-shaped cF_OF_1 dimer (Figure 4c, d, g). It might also indicate a possibility of another type of dimerization via F_1 part of cF_OF_1, which is schematically shown in Figure 4e, f, and might have already been observed in literature (Figure 4g).

Preprints (www.preprints.org) | NOT PEER-REVIEWED | Posted: 4 May 2023 doi:10.20944/preprints202305.0170.v1

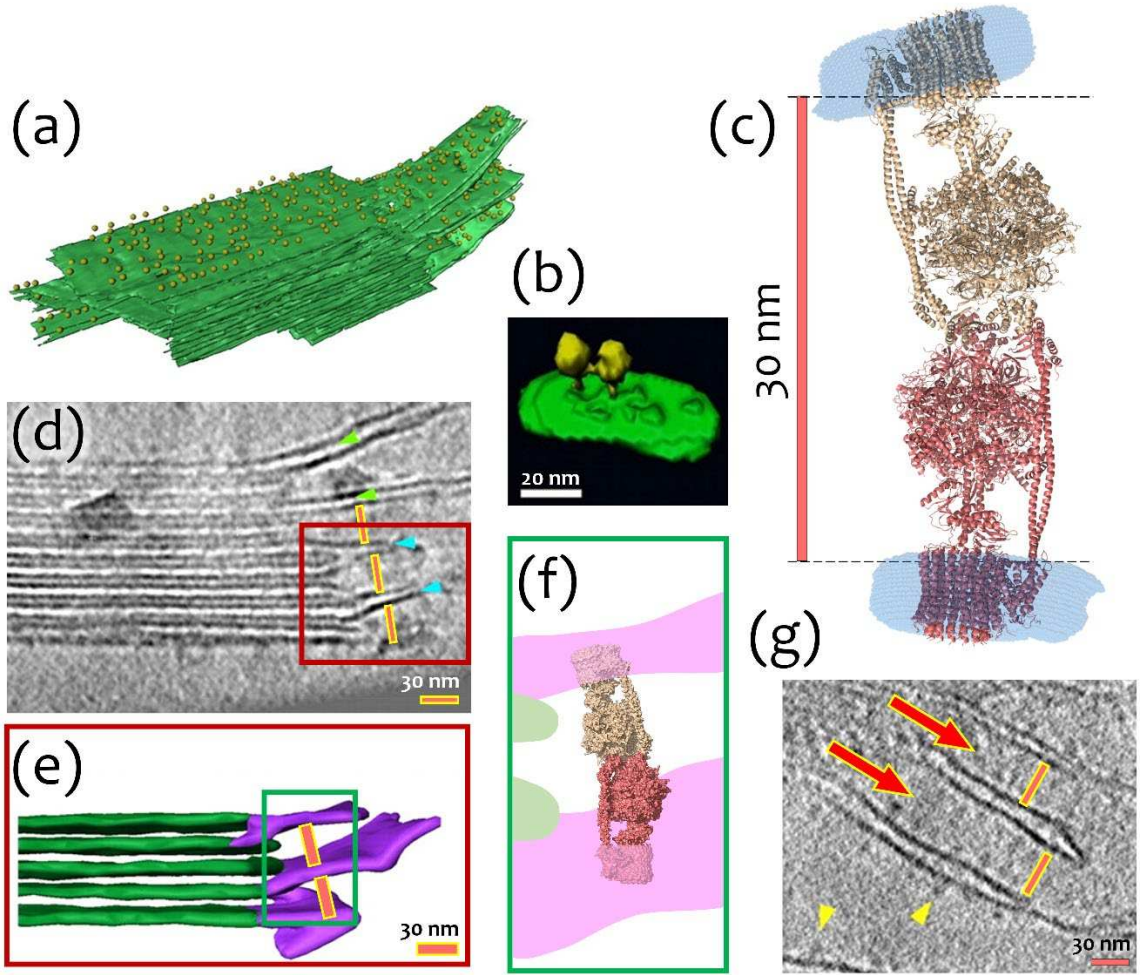

Figure 4. Possible biological interpretation of observed cFoF1 I-shaped dimer: (**a**) Segmented subvolume of a thylakoid stack with connected stroma lamellae, cFoF1 are shown as yellow 12-nm spheres, cFoF1 is randomly distributed over stromal lamellae; (**b**) Surface rendering of a lateral cFoF1 dimer in isolated pea thylakoid membranes; (**c**) A model of an I-shaped dimer with F1/F1 interaction interface, presumably via δ-subunit, the distance between membrane Fo parts of different cFoF1 monomers is about 30 nm; (**d**) Electron Tomography of Vitreous Spinach Chloroplast Sections, stacked grana and unstacked stroma thylakoid membranes are shown, the distance between neighboring stroma lamellae approximately fits the size of the I-shaped cFoF1 dimer; (**e**) Surface representation of connections between grana (green) and stroma (purple) thylakoids, the distance between neighboring stroma lamellae is about 30 nm; (**f**) Schematic representation of an I-shaped cFoF1 dimer in between of two neighboring stroma lamellae; (**g**) A part of a tomographic slice showing neighboring stroma lamellae, the distance between them approximately fits the size of an I-shaped ATP-synthase dimer. Presumably, ATP synthases shown with red arrows might be these I-shaped dimers. Panels (a), (b), (d), (e) and (g) were adapted from [3] with modifications.

3. Discussion

Studies of chloroplast ATP synthases already showed evidence of dimerization of cFoF1 from plant chloroplasts [3]. This dimerization is believed to be non-specific and is shown to be lateral, which means that two monomers of cFoF1 are interacting in one membrane. There is also evidence of cFoF1 dimers for single-cell green algae [18,19], however, the authors report only Blue Native PAGE and following SDS PAGE, therefore no structural data has been reported and the exact type of this interaction remains unclear.

Using SAXS studies of purified samples of cFoF1 from spinach chloroplasts we showed that the degree of oligomerization increases in response to changing of the NaCl concentration, both a

Preprints (www.preprints.org) | NOT PEER-REVIEWED | Posted: 4 May 2023 doi:10.20944/preprints202305.0170.v1

decrease and an increase from the point between 250 and 300 mM NaCl. where the dimeric fraction is minimal. We expected to obtain the model of lateral interaction similar to that reported in literature [3], but this model did not satisfy the distance between the two cF$_O$F$_1$ monomers (~200 Å). Thus, we came to a model with edge-to-edge interaction of two cF$_O$F$_1$, having an I-shape if visualizing a detergent belt at the membrane F$_O$ part of each monomer. Surprisingly, the model with F$_O$/F$_O$′ interaction did not fit well the experimental SAXS data (χ^2 = 2.3), although satisfied the distance between the two cF$_O$F$_1$ monomers, in contrast to the model with F$_1$/F$_1$′ interaction.

We showed the first structural evidence of the I-shaped type of dimerization of chloroplast F-ATP synthases from plants. Our model suggests F$_1$/F$_1$′ contacts between the cF$_O$F$_1$ monomers as it is shown by SAXS data approximation (χ^2 = 1.24) and it satisfies the value of the distance between the centers of masses of monomers D_{m-m} (eq. 1), which is about 200 Å. This means that the contacts between monomers of cF$_O$F$_1$ should be at the edge of the F$_1$ part to satisfy the conditions of comparatively large distance which is about the size of the whole protein complex cF$_O$F$_1$. Taken these facts together we hypothesize that the F$_1$/F$_1$′ contacts between cF$_O$F$_1$ monomers presumably might be via δ-subunit, which is at the top of the catalytic head ($\alpha_3\beta_3$) of the enzyme.

In order to check the possibility of the F$_1$/F$_1$ interaction we performed a macromolecular docking using HDOCK protein–protein docking web-server [15]. Considering δ-subunit as a key subunit for cF$_O$F$_1$ dimer formation (see *Macromolecular docking* section in Materials and Methods for the details) we obtained models of a dimer, which, in addition to contacts between δ-subunit, showed contacts between other subunits, including α-, β-, b- and b′-subunit. The resulting models can be assessed as reasonable both in terms of HDOCK confidence score values and parameters of macromolecular interfaces estimated using the PDBePISA web-server [16] (see Figure S4).

To understand which region(s) of a δ-subunit can potentially play a role in the I-shaped dimer formation, we evaluated intrinsic disorder propensity of this protein, since disordered regions are known to often contribute to the protein-protein interactions, being capable of undergoing binding-induced folding [20–23]. Furthermore, even when a crystal structure of a query protein is solved, one often can find noticeable levels of intrinsic disorder, since very significant fraction of proteins in PDB contains regions with missing electron density, which are potentially intrinsically disordered [24,25]. As we already indicated earlier [1], based on the analysis of the reported crystal structure of cF$_O$F$_1$ from the spinach chloroplasts (see PDB ID: 6FKF), each subunit of this protein contains regions of missing electron density, including the chain δ with residues 1-70 and 250-257. This indicates that very significant parts of each cF$_O$F$_1$ subunit are expected to be disordered even within the assembled complex [1]. The idea of the presence of significant levels of disorder in the cF$_O$F$_1$ δ-subunit is further supported by Figure 5a showing a model 3D-structure generated for the full-length δ-subunit by AlphaFold [26,27], which is the most accurate AI-based platform for the protein structure prediction [28] and Figure 5b representing the disorder profile of this protein generated based on the outputs of six commonly used disorder predictors from the PONDR family, such as PONDR® VLXT [29], PONDR® VL3 [30], PONDR® VLS2 [31], and PONDR® FIT [32], as well as IUPred2 (Short) and IUPred2 (Long) [33]. Figure 5 clearly shows that the long N-terminal region of the cF$_O$F$_1$ δ-subunit is expected to be highly disordered. Utilization of the flDPnn webserver that predicts disorder, disorder-based functions and disordered linkers [34], revealed that residues 1-3, 22-26, and 59-66 of the cF$_O$F$_1$ δ-subunit might be involved in the disorder-dependent protein-protein interactions.

Preprints (www.preprints.org) | NOT PEER-REVIEWED | Posted: 4 May 2023 doi:10.20944/preprints202305.0170.v1

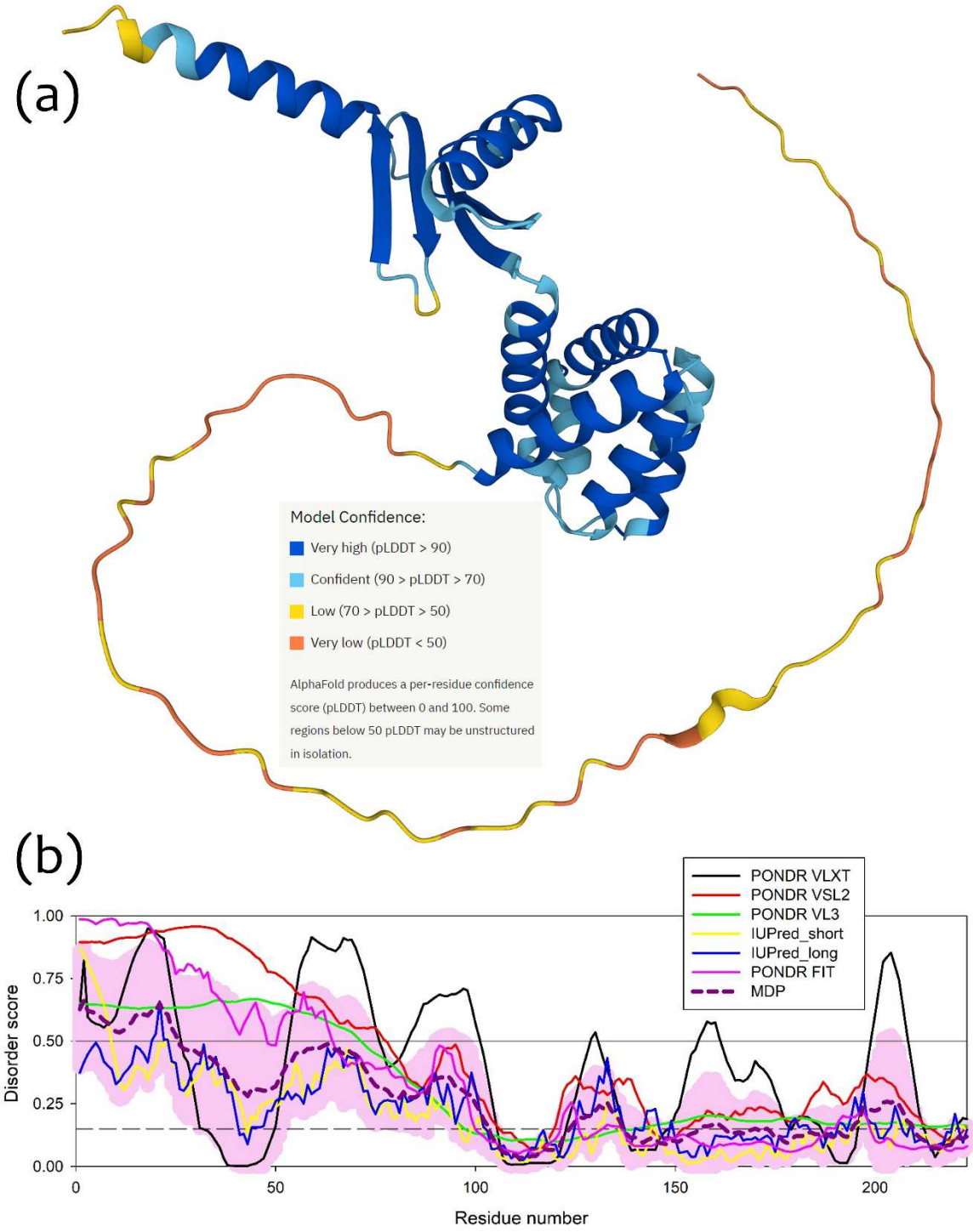

Figure 5. Structure and disorder in the cF$_O$F$_1$ δ-subunit: (**a**) 3D structure of the cF$_O$F$_1$ δ-subunit generated by AlphaFold2; (**b**) Per-residue intrinsic disorder predisposition of the cF$_O$F$_1$ δ-subunit from the spinach chloroplasts. Intrinsic disorder profile was generated using he outputs of the Rapid Intrinsic Disorder Analysis Online (RIDAO) platform [35] that aggregates the results from a number of well-known disorder predictors, such as PONDR® VLXT, PONDR® VL3, PONDR® VLS2, PONDR® FIT, and IUPred2 (Short) and IUPred2 (Long) and also produces the mean disorder profile (MDP) and corresponding error distribution (pink shadow). The outputs of the evaluation of the per-residue disorder propensity by these tools are represented as real numbers between 1 (ideal prediction of disorder) and 0 (ideal prediction of order). A threshold of 0.5 is used to identify disordered residues and regions in query proteins. Residues with the disorder scores (DS) $0.15 \leq DS < 0.5$ are considered

 doi:10.20944/preprints202305.0170.v1

as moderately disordered, residues with 0.25 ≤ DS < 0.5 are considered as moderately disordered, whereas residues with 0.15 ≤ DS < 0.25 are flexible.

We should notice that it is a big challenge to show directly the I-shaped structural organization of cF$_O$F$_1$ because of weak non-specific interactions between the cF$_O$F$_1$ monomers. For example, a recent study demonstrated a cryo-EM structure of the monomer of ATP synthase from spinach chloroplasts reconstituted into lipid nanodiscs [10]. However, the procedure of grid preparation could expose the sample to harsh conditions, which might break the F$_1$/F$_1$' contacts.

Another way of obtaining high-resolution structural information is protein crystallography. However, crystallization of ATP synthase as well as large membrane protein complexes is the key challenges in structural biology nowadays [1]. A crystallization by using lipid *in meso* phases (*in meso* method), e.g., lipid cubic phases (LCP), provides the crystals of membrane proteins in close to native conditions [36]. However, due to limitations of the diameters of LCP water channels the size of a water-exposed part of the protein complex is limited. Potentially perspective can be *in bicelles* crystallization [37,38], which was successfully applied for several membrane proteins with a large water-soluble part [39–41]. However, at the moment of this writing there is no reported successful cases of *in bicelles* crystallization of an ATP synthase.

ATP synthase crystallization by using vapor diffusion (VD) method, which allows avoiding the protein size limitations, has another problem connected with stabilization of membrane proteins in solution and fast kinetics of crystallization processes. Thus, crystal structures of almost full ATP synthase complexes were obtained only in several cases during the whole period of ATP synthase studies [42–47], which indicates a big challenge of obtaining crystals of ATP synthase. It is worth pointing out that even if a crystal of cF$_O$F$_1$ is grown it can also rearrange contacts between cF$_O$F$_1$ monomers.

In order to directly observe I-shaped dimerization we used SAXS method, which allowed us to obtain structural information in close to native conditions, allowing observing non-specifically connected cF$_O$F$_1$ monomers and obtaining the information about their supramolecular arrangement. SAXS does not require crystals or low temperatures, although in case of a mixture of monomers and oligomers SAXS data should be carefully analyzed [12,48].

In literature, there are debates about the possible physiological roles of dimers and higher oligomers of cF$_O$F$_1$ [3,49]. Some papers show evidence of the presence of dimers of cF$_O$F$_1$ in microorganisms [18,19,50]. Other papers claimed that these dimers might be only aggregates without specific structural arrangement or functional role [49,51]. Commonly, inhibition of ATP hydrolysis in chloroplasts occurs via a redox switch inserted into a γ-subunit of cF$_O$F$_1$ [10].

We hypothesize that the I-shaped type of dimerization might stabilize the stacks of thylakoids by possible connection of neighbor lamellae. This might be also connected with an increase of ionic strength in plant chloroplasts at dark [5,6]. Probably, formation of I-shaped dimers might establish an indirect interaction between lamellae (especially close to grana) and help to stabilize thylakoid stacks. Such dimers might be observed in more or less native conditions by cryo-electron tomography (Figure 4). However, reported structural studies of chloroplasts were made during the light phase [3,52], leaving a possibility to find native I-shaped dimers of cF$_O$F$_1$ in similar experiments at dark.

If an I-shaped dimer of cF$_O$F$_1$ exists in nature, we hypothesize that it might also represent a novel mechanism of a subtle regulation of ATP synthesis in plant chloroplasts and preventing ATP hydrolysis at dark periods. Increasing ionic strength in chloroplasts in the absence of light might trigger the formation of cF$_O$F$_1$ I-shaped dimers as well as pairs of cF$_O$F$_1$ observed in literature [3].

4. Materials and Methods

4.1. cF$_O$F$_1$ isolation and purification

The protein complex cF$_O$F$_1$ was isolated and purified from spinach chloroplasts as described [7,8] with minor modifications. Briefly, thylakoid membranes were solubilized in a buffer containing 60 mM n-Octyl-β-D-glucopyranoside and 25 mM Sodium Cholate v/v = 1/1, ultracentrifuged at 200 000

Preprints (www.preprints.org) | NOT PEER-REVIEWED | Posted: 4 May 2023 doi:10.20944/preprints202305.0170.v1

g for 1 h and a pellet was discarded. Then the solution underwent ammonium sulfate (AS) precipitation in the range of 1.2 – 1.8 M of AS. The precipitate at 1.8 M AS was either resuspended in a buffer containing ~2 mM tPCC-α-M, ultracentrifuged at 45 000 g and a pellet was discarded, a solution after 0.45 μm filtering was uploaded onto a column with POROS™ 20 HQ Strong Anion Exchange Resin and anion exchange chromatography was performed in a gradient of NaCl (50 – 1000 mM) in a buffer: 30 mM HEPES (pH 8.0), 2 mM $MgCl_2$, 0.04% (w/v) tPCC-α-M; or alternatively precipitate at 1.8 M AS was resuspended in a buffer containing 16 mM N-dodecyl β-D-maltoside (DDM), ultracentrifuged in a sucrose gradient (15 – 50 % w/v) at 200 000 g for 16 h, and the fraction between 29 and 36 % w/v of sucrose was desalted and underwent red-120 dye-ligand chromatography. Both methods provided ATP synthase applicable for further structural studies.

4.2. Blue Native Polyacrylamide Gel Electrophoresis

BN-PAGE was performed as described [53,54]. Briefly, the samples of cF_OF_1 were analysed in linear gradient polyacrylamide gel (from 4 to 14% (w/v) BN-PAGE, the separation gel was overlayed with an 3% (w/v) sample gel) (according 10.1080/13813455.2016.1218518, 10.1016/0003-2697(91)90094-A). An electrophoresis apparatus (SE 400, Cytiva) was used with cathode buffer contained 0.002% coomassie brilliant blue G-250 (Bio-Rad), phoresis duration was 16h. All native electrophoresis runs were performed at 100V and at 4°C. Hight molecular weight marker (HMW, #17044501, Cytiva) were used with the 10 ul load on a line.

4.3. Small-angle scattering measurements

SANS experiments were done on the YuMO spectrometer (IBR-2, Dubna, Russia) [55] with two-detector system [56,57]. For SANS measurements, two samples of cF_OF_1 were prepared. The first sample was obtained by anion-exchange chromatography (AEX). The second sample was obtained by dialysis of AEX-purified protein in 93% D_2O-buffer with 300 mM NaCl, 30 mM HEPES (pH ~8.0 [58]), 2 mM $MgCl_2$, 0.04 % (w/v) tPCC-α-M. Each sample (V = 400 uL) was poured into a Helma quartz cuvette (path length 1 mm) and placed to the temperature-controlled sample chamber [57] for further SANS measurements. Total exposure time for each sample was 80 min.

SAXS measurements were performed on the instrument Rigaku MicroMax-007 HF (MIPT, Dolgoprudny, Russia), which was used and described previously [38,59]. SAXS data were obtained for six samples of ATP synthase. First sample with protein concentration of ~5 mg/ml was obtained by purification using anion-exchange chromatography (see Figure 1). Other five samples were obtained by overnight dialysis in buffers containing 30 mM HEPES, 2 mM $MgCl_2$, 0.04% (w/v) tPCC-α-M, and different NaCl concentrations: 150, 250, 300, 350, and 450 mM. Each sample (V = 30 uL) was poured into a glass capillary, which was sealed by gas-burner or wax and placed into a vacuum chamber at a distance of 2.0 m from a multiwire gas-filled detector Rigaku ASM DTR Triton 200. All measurements were done at room temperature. A thermal stability of cF_OF_1 at room temperature was checked by Dynamic Scanning Fluorimetry (see the section *Dynamic Scanning Fluorimetry*). See Table S1 for other details of SAXS measurements and data treatment.

4.4. Small-angle scattering data treatment

In the case of SAXS data, first, SAXSGui software was used to convert 2D images of scattering intensity *vs* transmitted momentum in reciprocal space $Q = 4\pi \sin(\theta)/\lambda$ (where λ = 1.5405 Å (K_α of Cu), 2θ – a scattering angle) to 1D-profiles I(Q) by using a radially integration. For Q-calibration a powder of silver behenate (AgBh) was used (Q = 0.1076 $Å^{-1}$, d = 58.38 Å) [60]. In the case of SANS data, raw data were converted to one-dimensional data set I(Q) with a program SAS (version 5.1.5) [61]. Then, in both cases a regularized model fit of I(Q) 1D-profiles was used for calculation of a pair-distance distribution function P(R) by a program GNOM from ATSAS program package [62,63]. Visualizing of high-resolution models of cF_OF_1 dimers was done by PyMOL software [64]. MEMPROT software [11] was used to fit an experimental SAXS data for AEX-purified cF_OF_1 using a high-resolution model of cF_OF_1 from spinach chloroplasts (PDB ID: 6FKF) with a pseudo-atomic

 doi:10.20944/preprints202305.0170.v1

model of the detergent belt surrounding its transmembrane part. For proper orienting of the cF_OF_1 model before running MEMPROT (place the center of the transmembrane part at the origin (zero) and set the normal vector to the membrane plane along z-axis) we used a PPM web server [65]. A program OLIGOMER [66] from ATSAS was used to fit experimental SAXS data from a two-component mixture of monomers and dimers of cF_OF_1 and to obtain the volume fractions of each component in the mixture. A program CRYSOL [67] (command line mode) from ATSAS was used for evaluating the solution scattering from macromolecules in order to fit experimental SAXS data and/or prepare a set of form-factors for subsequent run of OLIGOMER program. See Table S1 for other details of SAXS measurements and data treatment.

4.5. Macromolecular docking

For validation of possible F_1/F_1 interaction of cF_OF_1 monomers we performed a macromolecular docking using HDOCK protein–protein docking web-server [68]. Considering δ-subunit as a key subunit for dimer formation observed by SAXS, we used the following residue distance restraints: 1-257:d 1-257:d 50. Here, letter "d" corresponds to δ-subunit chain, "1-257" are numbers that cover all residues presented in δ-subunit, and a number "50" corresponds to condition that residues 1-257 of a chain "d" on the receptor and on the ligand will be within 50 Å. Screening of the distance value in the range of 10 – 150 with a step = 10 shows the same docking results. Top 10 obtained HDOCK models, in addition to contacts between δ-subunit, demonstrated contacts between other subunits, including α, β, b and b', and shown the values of the HDOCK confidence score in the range 0.39 – 0.52 (Figure S4). Accordingly to the description of HDOCK it is considered that two molecules would be possible to bind, when the confidence score is between 0.5 and 0.7. However, taking into account the comment of the authors: "the confidence score here should be used carefully due to its empirical nature", the lower value of 0.5 is empirical and models with scores slightly below 0.5 can also be considered as possible and reasonble. Additionally, we checked the parameters of macromolecular dimerization interfaces using the PDBePISA web-server [16]. Results are shown in Figure S4.

In order to check the possibility of F_O/F_O interaction we also performed a macromolecular docking using HDOCK web-server. Considering c-subunit as a key subunit for dimer formation observed by SAXS, we used the residue distance restraints correspoding to 10 Å distance between residue 3 in c-subunits on the receptor and on the ligand (3:g 3:q 10). The only model that satisfies the condition $D_{m\text{-}m} \geq 201$ Å (eq. 1), has a high value of the HDOCK confidence score = 0.78 (Docking Score = -212.65), which corresponds to a high probability of the formation of such a contact. However, dimeriation via F_O/F_O interaction was not confirmed using SAXS data.

4.6. Dynamic Scanning Fluorimetry

We used Prometheus Panta from NanoTemper Technologies to check the thermostability of the protein complex cF_OF_1. Experiments were carried out in standard capillaries Prometheus NT.48 (Cat.# PR-C002). A temperature scan was conducted with 4 °C / min slope for temperature range 15 – 75 °C, an excitation LED power was 70 %. Thermal stability parameters (T_{onset}, T_m) were calculated by Panta.Analysis software (NanoTemper Technologies). Folding state transition was monitored by the ratio of fluorescence intensity at 330 nm and 350 nm as a function of temperature, where T_{onset} (onset temperature of thermal unfolding) was 51.6 °C and T_m (inflection temperature of thermal unfolding) was 66.9 °C (Figure S5). Thus, at 20°C a stability of the protein was not disrupted.

Supplementary Materials: The following supporting information can be downloaded at: Preprints.org, Figure S1: Characterization of the purified cF_OF_1 by BN-PAGE; Figure S2: SANS characterization of cF_OF_1; Figure S3: Influence of a detergent belt on quality of SAXS data approximation. Figure S4: Models of F_1/F_1-interface dimers of cF_OF_1 based on the top 10 HDOCK predictions; Figure S5: Thermal unfolding and refolding graphs measured by nanoDSF method; Table S1: SAXS experimental details and data evaluation summary.

Author Contributions: Conceptualization, A.V.V., Yu.L.R., N.A.D., and V.I.; methodology, A.V.V., Yu.L.R., and A.I.K.; software, E.V.Z., S.D.O., S.D.I., and A.V.M.; validation, S.D.O. and A.V.M.; formal analysis, Yu.L.R., S.D.O., A.V.M., and V.N.U.; investigation, A.V.V., Yu.L.R., M.Yu.N., S.D.O., D.P.V., V.V.S., D.D.K., Yu.S.S., Yu.A.Z., V.N.U., and I.S.O.; resources, A.V.V.; data curation, A.V.V., Yu.L.R., E.V.Z., and V.N.U.; writing—

original draft preparation, A.V.V. and Yu.L.R.; writing—review and editing, A.V.V., Yu.L.R., A.I.K., V.N.U., and V.I.; visualization, A.V.V., Yu.L.R., E.V.Z., S.D.O., V.V.S., V.N.U., and A.V.M.; supervision, A.V.V., N.A.D., A.I.K. and V.I.; project administration, A.V.V.; funding acquisition, A.V.V. All authors have read and agreed to the published version of the manuscript.

S.D.O. and Yu.L.R. contributed equally and either has the right to list himself first in bibliographic documents.

Funding: Protein purification, SAXS measurements and SAXS data analysis were done with the support from the Russian Science Foundation (RSF) Project 22-74-00044.

Yu.L.R. acknowledges the support from the Ministry of Science and Higher Education of the Russian Federation (agreement 075-03-2023-106, project FSMG-2021-0002).

Small-angle neutron scattering studies were supported by the Ministry of Science and Higher Education of the Russian Federation (Grant No. 075-15-2021-1354).

Data Availability Statement: SAXS data of cF$_O$F$_1$ at different NaCl concentrations are deposited in SASBDB with the IDs: SASxxxx(draft ID: 4860), SASxxxx(draft ID: 4861), SASxxxx(draft ID: 4862), SASxxxx(draft ID: 4863), SASxxxx(draft ID: 4864), SASxxxx(draft ID: 4865).

Acknowledgments: We acknowledge Frank Laboratory of Neutron Physics, Joint Institute for Nuclear Research, Dubna, Russia, for granting access to the small-angle neutron scattering spectrometer YuMO (IBR-2).

Conflicts of Interest: The authors declare no conflict of interest.

References

1. Vlasov, A. V; Osipov, S.D.; Bondarev, N.A.; Uversky, V.N.; Borshchevskiy, V.I.; Yanyushin, M.F.; Ilya, ·; Manukhov, V.; Rogachev, A. V; Vlasova, A.D.; et al. ATP Synthase FOF1 Structure, Function, and Structure-Based Drug Design. *Cellular and Molecular Life Sciences 2022 79:3* **2022**, *79*, 1–27, doi:10.1007/S00018-022-04153-0.
2. Kühlbrandt, W. Structure and Mechanisms of F-Type ATP Synthases. *Annu Rev Biochem* **2019**, *88*, 515–549, doi:10.1146/annurev-biochem-013118-110903.
3. Daum, B.; Nicastro, D.; Austin, J.; Richard McIntosh, J.; Kühlbrandt, W. Arrangement of Photosystem II and ATP Synthase in Chloroplast Membranes of Spinach and Pea. *Plant Cell* **2010**, *22*, 1299–1312, doi:10.1105/tpc.109.071431.
4. Robinson, S.P.; Downton, W.J.S. Potassium, Sodium, and Chloride Content of Isolated Intact Chloroplasts in Relation to Ionic Compartmentation in Leaves. *Arch Biochem Biophys* **1984**, *228*, 197–206, doi:10.1016/0003-9861(84)90061-4.
5. Chow, W.; Wagner, A.; Hope, A. Light-Dependent Redistribution of Ions in Isolated Spinach Chloroplasts. *Functional Plant Biology* **1976**, *3*, 853–861, doi:10.1071/PP9760853.
6. Nobel, P.S. Light-Induced Changes in the Ionic Content of Chloroplasts in Pisum Sativum. *Biochimica et Biophysica Acta (BBA) - Bioenergetics* **1969**, *172*, 134–143, doi:10.1016/0005-2728(69)90098-X.
7. Vlasov, A.V. New Structural Insights in Chloroplast F1FO-ATP Synthases - RWTH Publications, RWTH Aachen University, 2021.
8. Vlasov, A. V.; Kovalev, K. V.; Marx, S.-H.; Round, E.S.; Gushchin, I.Yu.; Polovinkin, V.A.; Tsoy, N.M.; Okhrimenko, I.S.; Borshchevskiy, V.I.; Büldt, G.D.; et al. Unusual Features of the C-Ring of F1FO ATP Synthases. *Sci Rep* **2019**, *9*, 18547, doi:10.1038/s41598-019-55092-z.
9. Balakrishna, A.M.; Seelert, H.; Marx, S.-H.; Dencher, N.A.; Grüber, G. Crystallographic Structure of the Turbine C-Ring from Spinach Chloroplast F-ATP Synthase. *Biosci Rep* **2014**, *34*, e00102, doi:10.1042/BSR20130114.
10. Hahn, A.; Vonck, J.; Mills, D.J.; Meier, T.; Kühlbrandt, W. Structure, Mechanism, and Regulation of the Chloroplast ATP Synthase. *Science* **2018**, *360*, eaat4318, doi:10.1126/science.aat4318.
11. Pérez, J.; Koutsioubas, A. Memprot: A Program to Model the Detergent Corona around a Membrane Protein Based on SEC-SAXS Data. *Acta Crystallogr D Biol Crystallogr* **2015**, *71*, 86–93, doi:10.1107/S1399004714016678.
12. Ryzhykau, Y.L.; Vlasov, A. V.; Orekhov, P.S.; Rulev, M.I.; Rogachev, A. V.; Vlasova, A.D.; Kazantsev, A.S.; Verteletskiy, D.P.; Skoi, V. V.; Brennich, M.E.; et al. Ambiguities in and Completeness of SAS Data Analysis of Membrane Proteins: The Case of the Sensory Rhodopsin II–Transducer Complex. *Acta Crystallogr D Struct Biol* **2021**, *77*, 1386–1400, doi:10.1107/s2059798321009542.
13. Ryzhykau, Y.L.; Orekhov, P.S.; Rulev, M.I.; Vlasov, A. v.; Melnikov, I.A.; Volkov, D.A.; Nikolaev, M.Yu.; Zabelskii, D. v.; Murugova, T.N.; Chupin, V. v.; et al. Molecular Model of a Sensor of Two-Component Signaling System. *Sci Rep* **2021**, *11*, 10774, doi:10.1038/s41598-021-89613-6.

14. Molodenskiy, D.S.; Svergun, D.I.; Mertens, H.D.T. MPBuilder: A PyMOL Plugin for Building and Refinement of Solubilized Membrane Proteins Against Small Angle X-Ray Scattering Data. *J Mol Biol* **2021**, *433*, 166888, doi:10.1016/J.JMB.2021.166888.
15. Yan, Y.; Tao, H.; He, J.; Huang, S.Y. The HDOCK Server for Integrated Protein–Protein Docking. *Nature Protocols 2020 15:5* **2020**, *15*, 1829–1852, doi:10.1038/s41596-020-0312-x.
16. Krissinel, E.; Henrick, K. Inference of Macromolecular Assemblies from Crystalline State. *J Mol Biol* **2007**, *372*, 774–797, doi:10.1016/J.JMB.2007.05.022.
17. Minges, A.; Groth, G. Structure and Supramolecular Architecture of Chloroplast ATP Synthase. *Adv Bot Res* **2020**, *96*, 27–74, doi:10.1016/BS.ABR.2020.07.004.
18. Rexroth, S.; Meyer Zu Tittingdorf, J.M.W.; Schwaßmann, H.J.; Krause, F.; Seelert, H.; Dencher, N.A. Dimeric H+-ATP Synthase in the Chloroplast of Chlamydomonas Reinhardtii. *Biochim Biophys Acta Bioenerg* **2004**, *1658*, 202–211, doi:10.1016/j.bbabio.2004.05.014.
19. Schwaßmann, H.J.; Rexroth, S.; Seelert, H.; Dencher, N.A. Metabolism Controls Dimerization of the Chloroplast FoF1 ATP Synthase in Chlamydomonas Reinhardtii. *FEBS Lett* **2007**, *581*, 1391–1396, doi:10.1016/j.febslet.2007.02.057.
20. Disfani, F.M.; Hsu, W.-L.; Mizianty, M.J.; Oldfield, C.J.; Xue, B.; Dunker, A.K.; Uversky, V.N.; Kurgan, L. MoRFpred, a Computational Tool for Sequence-Based Prediction and Characterization of Short Disorder-to-Order Transitioning Binding Regions in Proteins. *Bioinformatics* **2012**, *28*, i75-83, doi:10.1093/bioinformatics/bts209.
21. Cheng, Y.; Oldfield, C.J.; Meng, J.; Romero, P.; Uversky, V.N.; Dunker, A.K. Mining Alpha-Helix-Forming Molecular Recognition Features with Cross Species Sequence Alignments. *Biochemistry* **2007**, *46*, 13468–13477, doi:10.1021/bi7012273.
22. Oldfield, C.J.; Cheng, Y.; Cortese, M.S.; Romero, P.; Uversky, V.N.; Dunker, A.K. Coupled Folding and Binding with Alpha-Helix-Forming Molecular Recognition Elements. *Biochemistry* **2005**, *44*, 12454–12470, doi:10.1021/bi050736e.
23. Garner, E.; Romero, P.; Dunker, A.; Brown, C.; Obradovic, Z. Predicting Binding Regions within Disordered Proteins. *Genome Inform Ser Workshop Genome Inform* **1999**, *10*, 41–50.
24. DeForte, S.; Uversky, V.N. Resolving the Ambiguity: Making Sense of Intrinsic Disorder When PDB Structures Disagree. *Protein Sci* **2016**, *25*, 676–688, doi:10.1002/pro.2864.
25. Le Gall, T.; Romero, P.R.; Cortese, M.S.; Uversky, V.N.; Dunker, A.K. Intrinsic Disorder in the Protein Data Bank. *J Biomol Struct Dyn* **2007**, *24*, 325–342, doi:10.1080/07391102.2007.10507123.
26. Varadi, M.; Anyango, S.; Deshpande, M.; Nair, S.; Natassia, C.; Yordanova, G.; Yuan, D.; Stroe, O.; Wood, G.; Laydon, A.; et al. AlphaFold Protein Structure Database: Massively Expanding the Structural Coverage of Protein-Sequence Space with High-Accuracy Models. *Nucleic Acids Res* **2022**, *50*, D439–D444, doi:10.1093/nar/gkab1061.
27. Jumper, J.; Evans, R.; Pritzel, A.; Green, T.; Figurnov, M.; Ronneberger, O.; Tunyasuvunakool, K.; Bates, R.; Žídek, A.; Potapenko, A.; et al. Highly Accurate Protein Structure Prediction with AlphaFold. *Nature* **2021**, *596*, 583–589, doi:10.1038/s41586-021-03819-2.
28. Kryshtafovych, A.; Schwede, T.; Topf, M.; Fidelis, K.; Moult, J. Critical Assessment of Methods of Protein Structure Prediction (CASP)-Round XIV. *Proteins* **2021**, *89*, 1607–1617, doi:10.1002/prot.26237.
29. Romero, P.; Obradovic, Z.; Li, X.; Garner, E.C.; Brown, C.J.; Dunker, A.K. Sequence Complexity of Disordered Protein. *Proteins* **2001**, *42*, 38–48, doi:10.1002/1097-0134(20010101)42:1<38::aid-prot50>3.0.co;2-3.
30. Peng, K.; Radivojac, P.; Vucetic, S.; Dunker, A.K.; Obradovic, Z. Length-Dependent Prediction of Protein Intrinsic Disorder. *BMC Bioinformatics* **2006**, *7*, 208, doi:10.1186/1471-2105-7-208.
31. Peng, K.; Vucetic, S.; Radivojac, P.; Brown, C.J.; Dunker, A.K.; Obradovic, Z. Optimizing Long Intrinsic Disorder Predictors with Protein Evolutionary Information. *J Bioinform Comput Biol* **2005**, *3*, 35–60, doi:10.1142/s0219720005000886.
32. Xue, B.; Dunbrack, R.L.; Williams, R.W.; Dunker, A.K.; Uversky, V.N. PONDR-FIT: A Meta-Predictor of Intrinsically Disordered Amino Acids. *Biochim Biophys Acta* **2010**, *1804*, 996–1010, doi:10.1016/j.bbapap.2010.01.011.
33. Mészáros, B.; Erdos, G.; Dosztányi, Z. IUPred2A: Context-Dependent Prediction of Protein Disorder as a Function of Redox State and Protein Binding. *Nucleic Acids Res* **2018**, *46*, W329–W337, doi:10.1093/nar/gky384.
34. Hu, G.; Katuwawala, A.; Wang, K.; Wu, Z.; Ghadermarzi, S.; Gao, J.; Kurgan, L. flDPnn: Accurate Intrinsic Disorder Prediction with Putative Propensities of Disorder Functions. *Nat Commun* **2021**, *12*, 4438, doi:10.1038/s41467-021-24773-7.
35. Dayhoff, G.W.; Uversky, V.N. Rapid Prediction and Analysis of Protein Intrinsic Disorder. *Protein Sci* **2022**, *31*, e4496, doi:10.1002/pro.4496.
36. Caffrey, M.; Cherezov, V. Crystallizing Membrane Proteins Using Lipidic Mesophases. *Nat Protoc* **2009**, *4*, 706–731, doi:10.1038/nprot.2009.31.

37. Faham, S.; Bowie, J.U. Bicelle Crystallization: A New Method for Crystallizing Membrane Proteins Yields a Monomeric Bacteriorhodopsin Structure. *J Mol Biol* **2002**, *316*, 1–6, doi:10.1006/JMBI.2001.5295.
38. Murugova, T.N.; Ivankov, O.I.; Ryzhykau, Y.L.; Soloviov, D. V.; Kovalev, K. V.; Skachkova, D. V.; Round, A.; Baeken, C.; Ishchenko, A. V.; Volkov, O.A.; et al. Mechanisms of Membrane Protein Crystallization in 'Bicelles.' *Scientific Reports 2022 12:1* **2022**, *12*, 1–17, doi:10.1038/s41598-022-13945-0.
39. Morgan, J.L.W.; McNamara, J.T.; Zimmer, J. Mechanism of Activation of Bacterial Cellulose Synthase by Cyclic Di-GMP. *Nature Structural & Molecular Biology 2014 21:5* **2014**, *21*, 489–496, doi:10.1038/nsmb.2803.
40. Noinaj, N.; Kuszak, A.J.; Gumbart, J.C.; Lukacik, P.; Chang, H.; Easley, N.C.; Lithgow, T.; Buchanan, S.K. Structural Insight into the Biogenesis of β-Barrel Membrane Proteins. *Nature 2013 501:7467* **2013**, *501*, 385–390, doi:10.1038/nature12521.
41. Lin, D.Y.W.; Huang, S.; Chen, J. Crystal Structures of a Polypeptide Processing and Secretion Transporter. *Nature 2015 523:7561* **2015**, *523*, 425–430, doi:10.1038/nature14623.
42. Stock, D.; Leslie, A.G.W.; Walker, J.E. Molecular Architecture of the Rotary Motor in ATP Synthase. *Science (1979)* **1999**, *286*, 1700–1705, doi:10.1126/science.286.5445.1700.
43. Dautant, A.; Velours, J.; Giraud, M.F. Crystal Structure of the Mg·ADP-Inhibited State of the Yeast F 1c10-ATP Synthase. *Journal of Biological Chemistry* **2010**, *285*, 29502–29510, doi:10.1074/jbc.M110.124529.
44. Watt, I.N.; Montgomery, M.G.; Runswick, M.J.; Leslie, A.G.W.; Walker, J.E. Bioenergetic Cost of Making an Adenosine Triphosphate Molecule in Animal Mitochondria. *Proc Natl Acad Sci U S A* **2010**, *107*, 16823–16827, doi:10.1073/pnas.1011099107.
45. Giraud, M.F.; Paumard, P.; Sanchez, C.; Brèthes, D.; Velours, J.; Dautant, A. Rotor Architecture in the Yeast and Bovine F 1-c-Ring Complexes of F-ATP Synthase. *J Struct Biol* **2012**, *177*, 490–497, doi:10.1016/j.jsb.2011.10.015.
46. Morales-Rios, E.; Montgomery, M.G.; Leslie, A.G.W.; Walker, J.E. Structure of ATP Synthase from Paracoccus Denitrificans Determined by X-Ray Crystallography at 4.0 Å Resolution. *Proc Natl Acad Sci U S A* **2015**, *112*, 13231–13236, doi:10.1073/pnas.1517542112.
47. Hahn, A.; Parey, K.; Bublitz, M.; Mills, D.J.; Zickermann, V.; Vonck, J.; Kühlbrandt, W.; Meier, T. Structure of a Complete ATP Synthase Dimer Reveals the Molecular Basis of Inner Mitochondrial Membrane Morphology. *Mol Cell* **2016**, *63*, 445–456, doi:10.1016/J.MOLCEL.2016.05.037.
48. Zabelskii, D.V.; Vlasov, A.V.; Ryzhykau, Y.L.; Murugova, T.N.; Brennich, M.; Soloviov, D.V.; Ivankov, O.I.; Borshchevskiy, V.I.; Mishin, A.V.; Rogachev, A.V.; et al. Ambiguities and Completeness of SAS Data Analysis: Investigations of Apoferritin by SAXS/SANS EID and SEC-SAXS Methods. In Proceedings of the Journal of Physics: Conference Series; 2018; Vol. 994.
49. Böttcher, B.; Gräber, P. The Structure of the H+-ATP Synthase from Chloroplasts and Its Subcomplexes as Revealed by Electron Microscopy. *Biochim Biophys Acta Bioenerg* 2000, *1458*, 404–416.
50. Vlasov, A.V.; Kovalev, Y.S.; Utrobin, P.K.; Ryzhykau, Y.L.; Frolov, F.V.; Zinovev, E.V.; Rogachev, A.V.; Kuklin, A.I.; Gordeliy, V.I. Photo-Voltage of Highly-Oriented Bacteriorhodopsin in Purple Membranes: Possibilities for Bio Solar Cells. *Optoelectronics and Advanced Materials, Rapid Communications* **2017**, *11*.
51. Daum, B.; Nicastro, D.; Austin, J.; Richard McIntosh, J.; Kühlbrandt, W. Arrangement of Photosystem II and ATP Synthase in Chloroplast Membranes of Spinach and Pea. *Plant Cell* **2010**, *22*, 1299–1312, doi:10.1105/tpc.109.071431.
52. Engel, B.D.; Schaffer, M.; Cuellar, L.K.; Villa, E.; Plitzko, J.M.; Baumeister, W. Native Architecture of the Chlamydomonas Chloroplast Revealed by in Situ Cryo-Electron Tomography. *Elife* **2015**, *2015*, doi:10.7554/ELIFE.04889.
53. Schägger, H.; von Jagow, G. Blue Native Electrophoresis for Isolation of Membrane Protein Complexes in Enzymatically Active Form. *Anal Biochem* **1991**, *199*, 223–231, doi:10.1016/0003-2697(91)90094-A.
54. Džinić, T.; Hartwig, S.; Lehr, S.; Dencher, N.A. Oxygen and Differentiation Status Modulate the Effect of X-Ray Irradiation on Physiology and Mitochondrial Proteome of Human Neuroblastoma Cells. *http://dx.doi.org/10.1080/13813455.2016.1218518* **2016**, *122*, 257–265, doi:10.1080/13813455.2016.1218518.
55. Kuklin, A.I.; Ivankov, O.I.; Rogachev, A. V.; Soloviov, D. V.; Islamov, A.K.; Skoi, V. V.; Kovalev, Y.S.; Vlasov, A. V.; Ryzhykau, Y.L.; Soloviev, A.G.; et al. Small-Angle Neutron Scattering at the Pulsed Reactor IBR-2: Current Status and Prospects. *Crystallography Reports 2021 66:2* **2021**, *66*, 231–241, doi:10.1134/S1063774521020085.
56. Kuklin, A.I.; Islamov, A.K.; Gordeliy, V.I. Scientific Reviews: Two-Detector System for Small-Angle Neutron Scattering Instrument. *Neutron News* **2005**, *16*, 16–18, doi:10.1080/10448630500454361.
57. Kuklin, A.I.; Soloviov, D. V; Rogachev, A. V; Utrobin, P.K.; Kovalev, Y.S.; Balasoiu, M.; Ivankov, O.I.; Sirotin, A.P.; Murugova, T.N.; Petukhova, T.B.; et al. New Opportunities Provided by Modernized Small-Angle Neutron Scattering Two-Detector System Instrument (YuMO). *J Phys Conf Ser* **2011**, *291*, 012013, doi:10.1088/1742-6596/291/1/012013.
58. Covington, A.K.; Paabo, M.; Robinson, R.A.; Bates, R.G. Use of the Glass Electrode in Deuterium Oxide and the Relation between the Standardized PD (PaD) Scale and the Operational PH in Heavy Water. *Anal Chem* **1968**, *40*, 700–706, doi:10.1021/AC60260A013/ASSET/AC60260A013.FP.PNG_V03.

59. Tsoraev, G. V.; Protasova, E.A.; Klimanova, E.A.; Ryzhykau, Y.L.; Kuklin, A.I.; Semenov, Y.S.; Ge, B.; Li, W.; Qin, S.; Friedrich, T.; et al. Anti-Stokes Fluorescence Excitation Reveals Conformational Mobility of the C-Phycocyanin Chromophores. *Structural Dynamics* **2022**, *9*, 054701, doi:10.1063/4.0000164.
60. Nyam-Osor, M.; Soloviov, D. V; Kovalev, Y.S.; Zhigunov, A.; Rogachev, A. V; Ivankov, O.I.; Erhan, R. V; Kuklin, A.I. Silver Behenate and Silver Stearate Powders for Calibration of SAS Instruments. *J Phys Conf Ser* **2012**, *351*, 012024, doi:10.1088/1742-6596/351/1/012024.
61. Soloviev, A.G.; Solovjeva, T.M.; Ivankov, O.I.; Soloviov, D. V.; Rogachev, A. V.; Kuklin, A.I. SAS Program for Two-Detector System: Seamless Curve from Both Detectors. *J Phys Conf Ser* **2017**, *848*, 012020, doi:10.1088/1742-6596/848/1/012020.
62. Manalastas-Cantos, K.; Konarev, P. V.; Hajizadeh, N.R.; Kikhney, A.G.; Petoukhov, M. V.; Molodenskiy, D.S.; Panjkovich, A.; Mertens, H.D.T.; Gruzinov, A.; Borges, C.; et al. ATSAS 3.0: Expanded Functionality and New Tools for Small-Angle Scattering Data Analysis. *urn:issn:1600-5767* **2021**, *54*, 343–355, doi:10.1107/S1600576720013412.
63. Franke, D.; Petoukhov, M. V.; Konarev, P. V.; Panjkovich, A.; Tuukkanen, A.; Mertens, H.D.T.; Kikhney, A.G.; Hajizadeh, N.R.; Franklin, J.M.; Jeffries, C.M.; et al. ATSAS 2.8: A Comprehensive Data Analysis Suite for Small-Angle Scattering from Macromolecular Solutions. *J Appl Crystallogr* **2017**, *50*, 1212–1225, doi:10.1107/S1600576717007786.
64. DeLano, W.L. Pymol: An Open-Source Molecular Graphics Tool. *CCP4 Newsletter on protein crystallography* **2002**, *40*, 82–92.
65. Lomize, M.A.; Pogozheva, I.D.; Joo, H.; Mosberg, H.I.; Lomize, A.L. OPM Database and PPM Web Server: Resources for Positioning of Proteins in Membranes. *Nucleic Acids Res* **2012**, *40*, D370–D376, doi:10.1093/nar/gkr703.
66. Konarev, P. V.; Volkov, V. V.; Sokolova, A. V.; Koch, M.H.J.; Svergun, D.I. PRIMUS: A Windows PC-Based System for Small-Angle Scattering Data Analysis. *urn:issn:0021-8898* **2003**, *36*, 1277–1282, doi:10.1107/S0021889803012779.
67. Svergun, D.I.; IUCr Determination of the Regularization Parameter in Indirect-Transform Methods Using Perceptual Criteria. *urn:issn:0021-8898* **1992**, *25*, 495–503, doi:10.1107/S0021889892001663.
68. Ferrè, F.; Clote, P. DiANNA: A Web Server for Disulfide Connectivity Prediction. *Nucleic Acids Res* **2005**, *33*, W230–W232, doi:10.1093/NAR/GKI412.